Biophysical Journal, Volume 97

Supporting Material

Molecular modeling of the misfolded insulin subunit and amyloid fibril

Jay H. Choi, Barnaby C. H. May, Holger Wille, and Fred E. Cohen

Supplementary Material

Molecular modeling of the misfolded insulin subunit and amyloid fibril

Jay H. Choi[*], Barnaby C. H. May[†,§], Holger Wille[†,§], and Fred E. Cohen[*,‡]

Departments of *Cellular and Molecular Pharmacology, [†]Neurology, [‡]Biochemistry and Biophysics, and [§]Institute for Neurodegenerative Diseases, University of California, San Francisco, CA 94158

Correspondence to: Fred E. Cohen, UCSF MC 2240, Genentech Hall, Room N472J, 600 16th Street, San Francisco, CA 94158-2517; Tel: (415) 743-1559; Fax: (415) 743-1685; E-mail: cohen@cmpharm.ucsf.edu.

Contents: Table S1, Figure S1, Figure S2, Figure S3, Figure S4, Figure S5, Figure S6, Figure S7, Table S2, Table S3, Figure S8, and Methods.

1. Supplementary Table 1

Table S1. Structural statistics from the MD simulation of the β-roll and β-helix insulin models.

A. Average backbone RMSD with respect to the starting structures[a] (Å)

	300 K	345 K	375 K
β-roll model	2.90 (0.17)	3.28 (0.37)	4.37 (0.51)
β-helix model	3.37 (0.37)	5.27 (0.53)	6.98 (0.86)

B. Average change in interchain backbone-backbone hydrogen bonds[b]

	300K	345 K	375 K
β-roll model	2.1 (0.3)	2.6 (0.3)	3.9 (1.2)
β-helix model	1.1 (0.1)	2.6 (0.9)	5.0 (1.0)

Values are reported as mean (S.D.) of three independent MD simulations. [a]Backbone RMSDs were calculated with respect to the initial structures, averaged over the 35-40 ns interval of the MD trajectories. [b]Average change in hydrogen bonds were calculated by subtracting the average number of hydrogen bonds over the 35-40 ns interval of the MD trajectories from the number of hydrogen bonds in initial structures.

2. Supplementary Figure 1

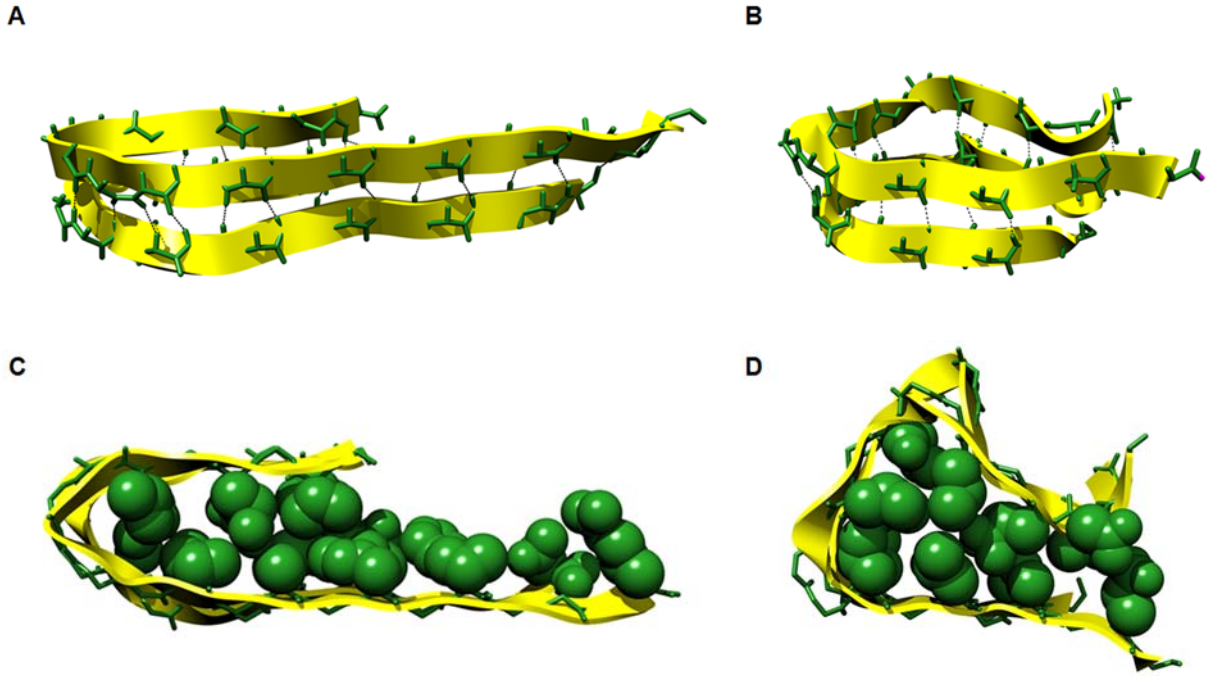

Figure S1. Structure of β-solenoid–based monomeric subunit models for the insulin amyloid fibril with proposed interchain hydrogen bonds and hydrophobic core packing. (**A**) The β-roll model with interchain backbone-backbone hydrogen bonds. (**B**) The β-helix model with interchain backbone-backbone hydrogen bonds. (C) The β-roll insulin monomeric subunit model with hydrophobic core packing. (D) The β-helix insulin monomeric subunit model with hydrophobic core packing. The interchain hydrogen bonds are shown as dashed lines, and hydrophobic core residue side-chains are shown as space filling models.

3. Supplementary Figure 2

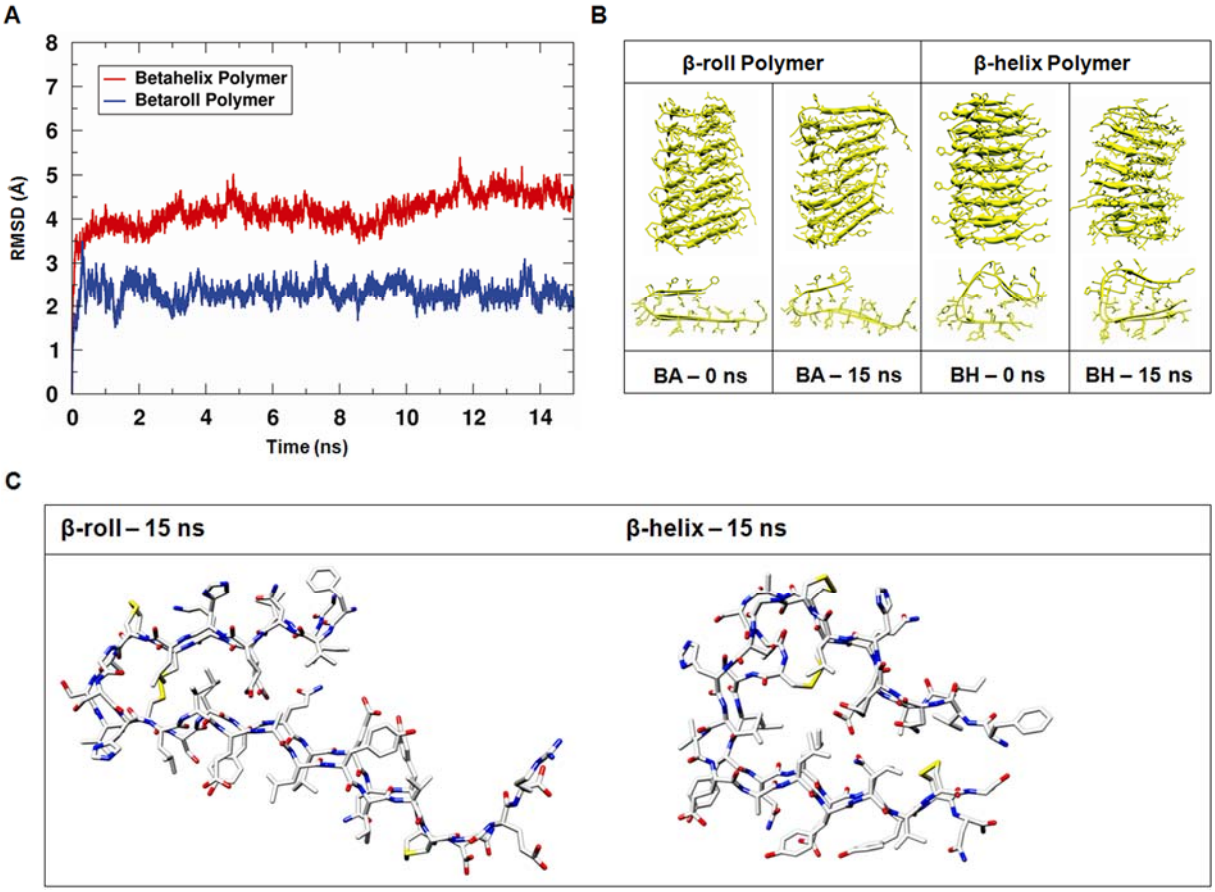

Figure S2. Molecular dynamics simulation of the β-roll and β-helix polymer models at 345 K under acidic conditions. (**A**) Backbone RMSDs of the β-roll model and β-helix polymer model relative to their initial structures as a function of simulation time are shown in blue and red respectively. (**B**) The initial and final structures of the β-roll model and β-helix polymer models are shown with the cross-sectional views of the third unit (from the top) of the polymeric constructs. (**C**) Cross-sectional view of the third units from the β-roll and β-helix based polymer models after 15 ns of MD simulation.

4. Supplementary Figure 3

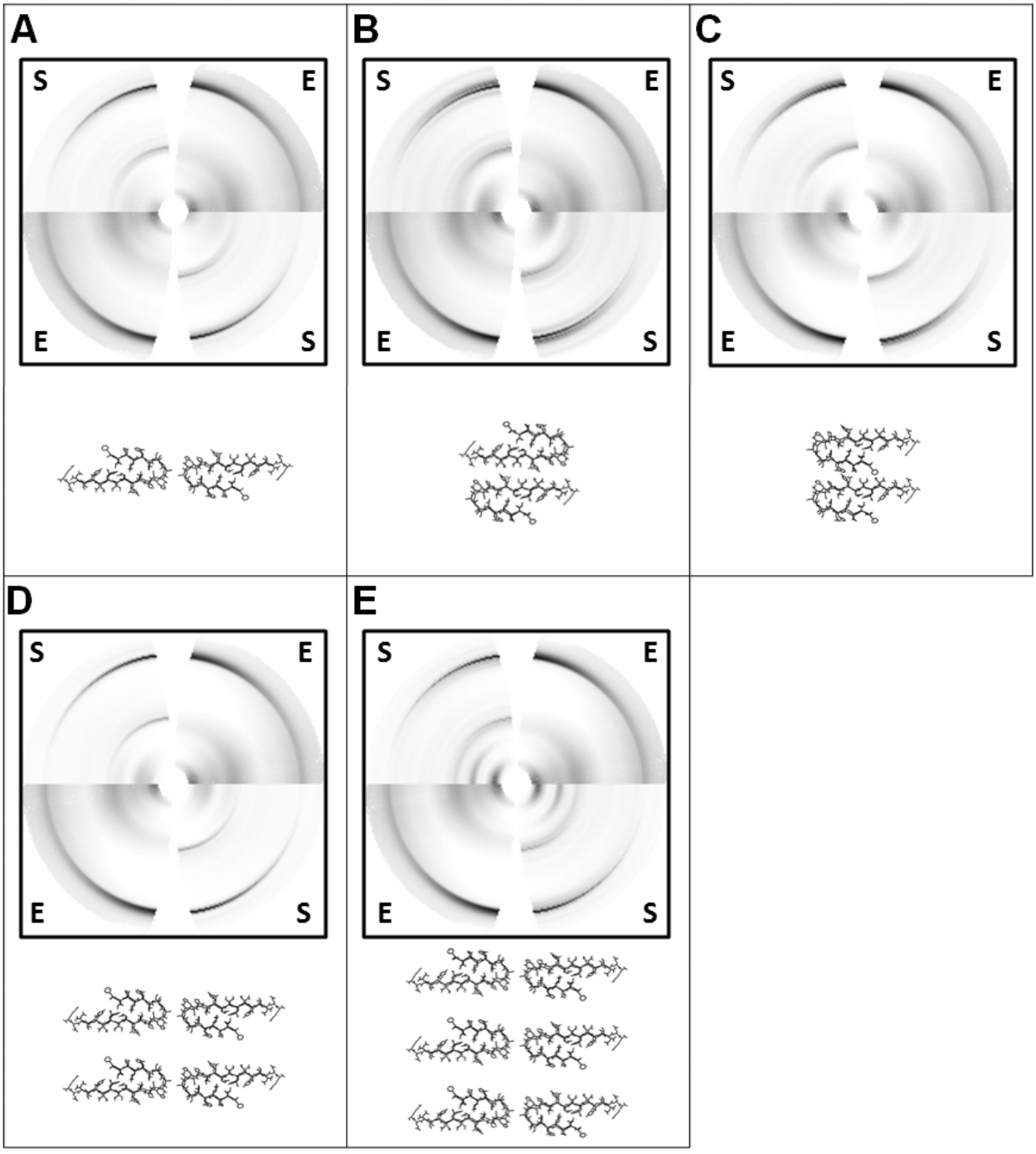

Figure S3. Experimental diffraction pattern of an insulin amyloid fibril and simulated diffraction patterns of β-roll–based twisted stack fibril models. (**A-E**) Each panel shows the cross-section of a model with a quadrant view of the experimental insulin X-ray fiber diffraction pattern (E) and the simulated fiber diffraction pattern (S).

5. Supplementary Figure 4

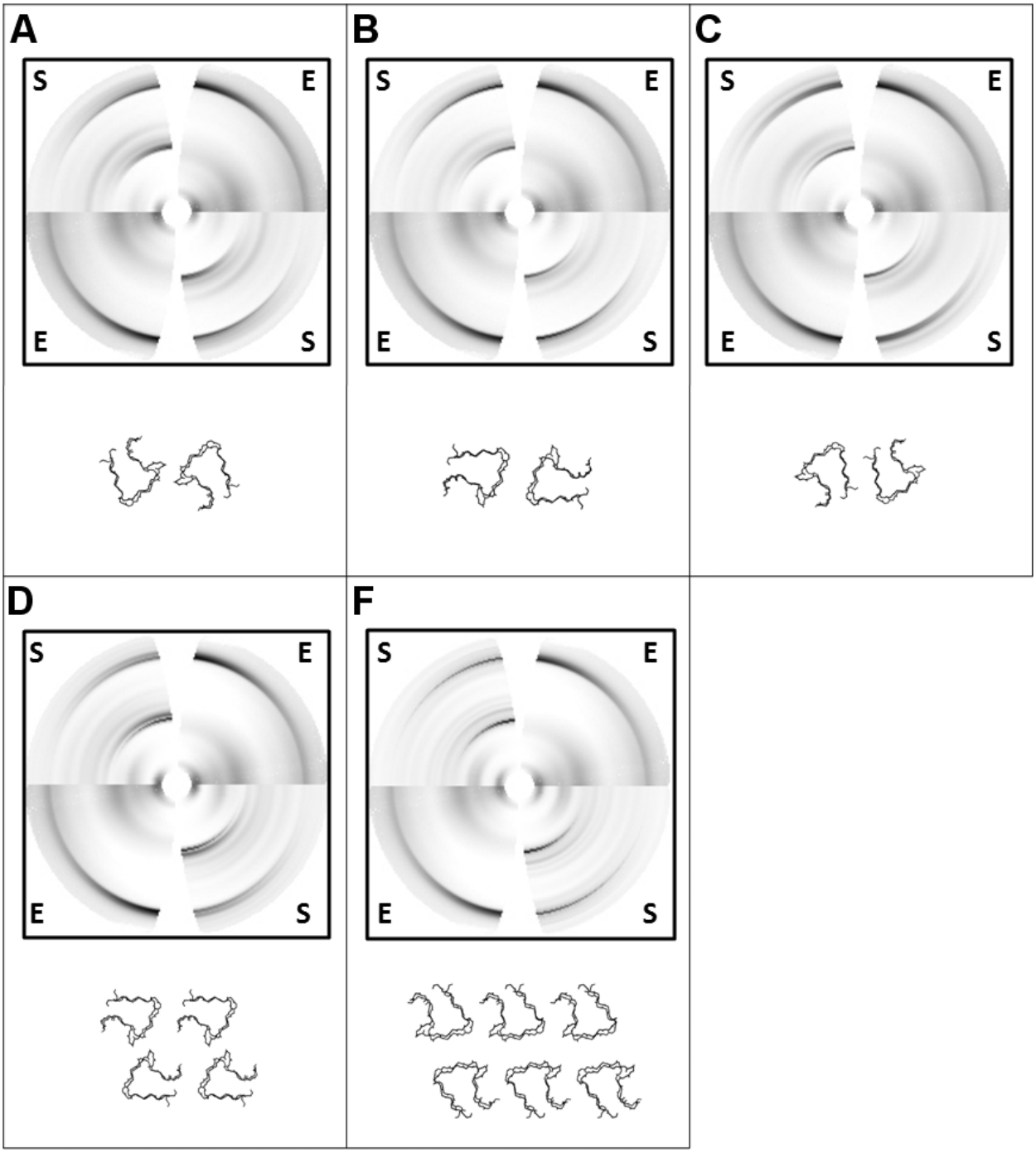

Figure S4. Experimental diffraction pattern of an insulin amyloid fibril and simulated diffraction patterns of β-helix–based twisted stack fibril models. (**A-E**) Each panel shows the cross-section of a model with a quadrant view of the experimental insulin X-ray fiber diffraction pattern (E) and the simulated fiber diffraction pattern (S).

6. Supplementary Figure 5

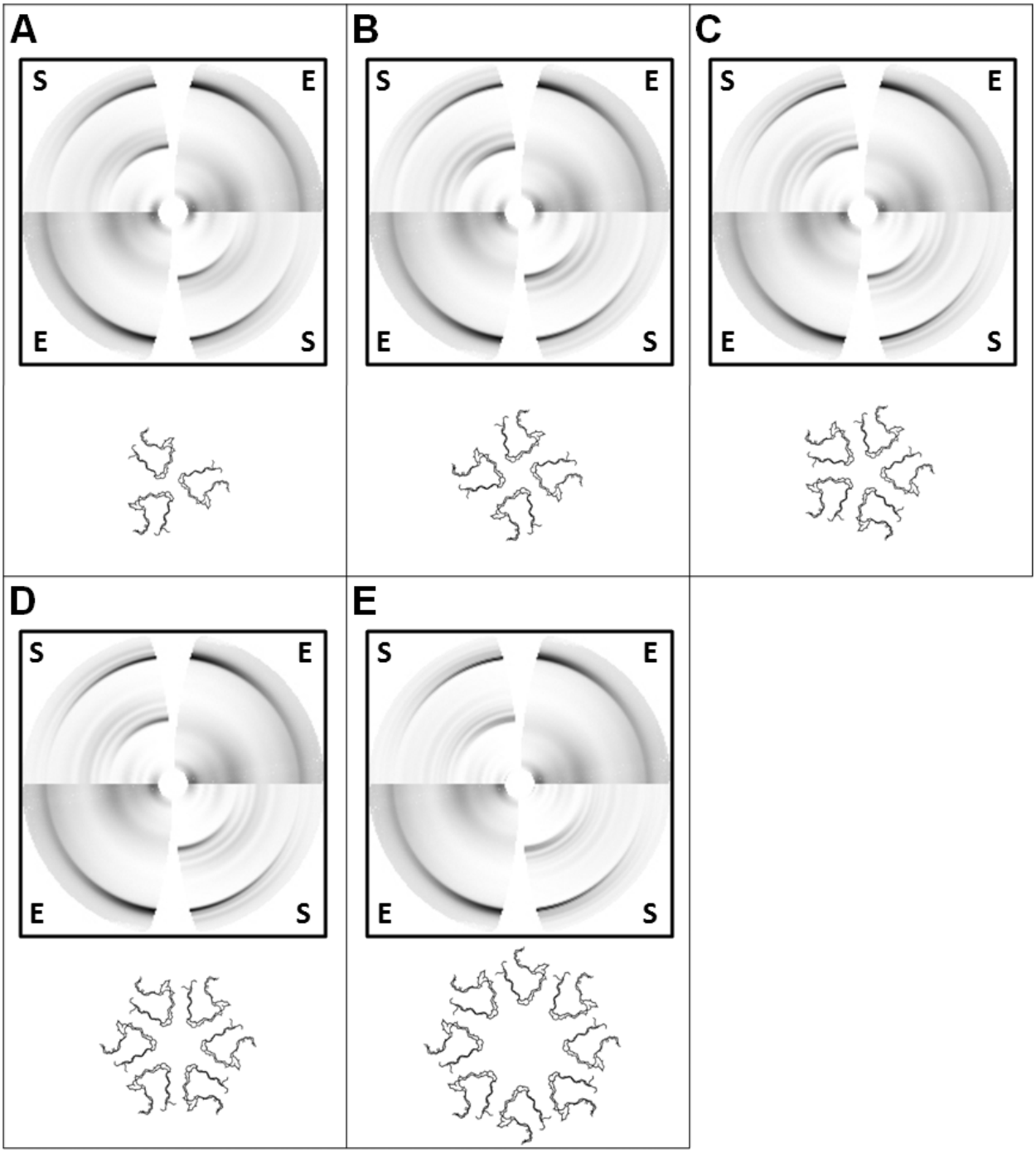

Figure S5. Experimental diffraction pattern of an insulin amyloid fibril and simulated diffraction patterns of β-helix–based helical fibril models. (**A**-**E**) Each panel shows the cross-section of a model with a quadrant view of the experimental insulin X-ray fiber diffraction pattern (E) and the simulated fiber diffraction pattern (S).

7. Supplementary Figure 6

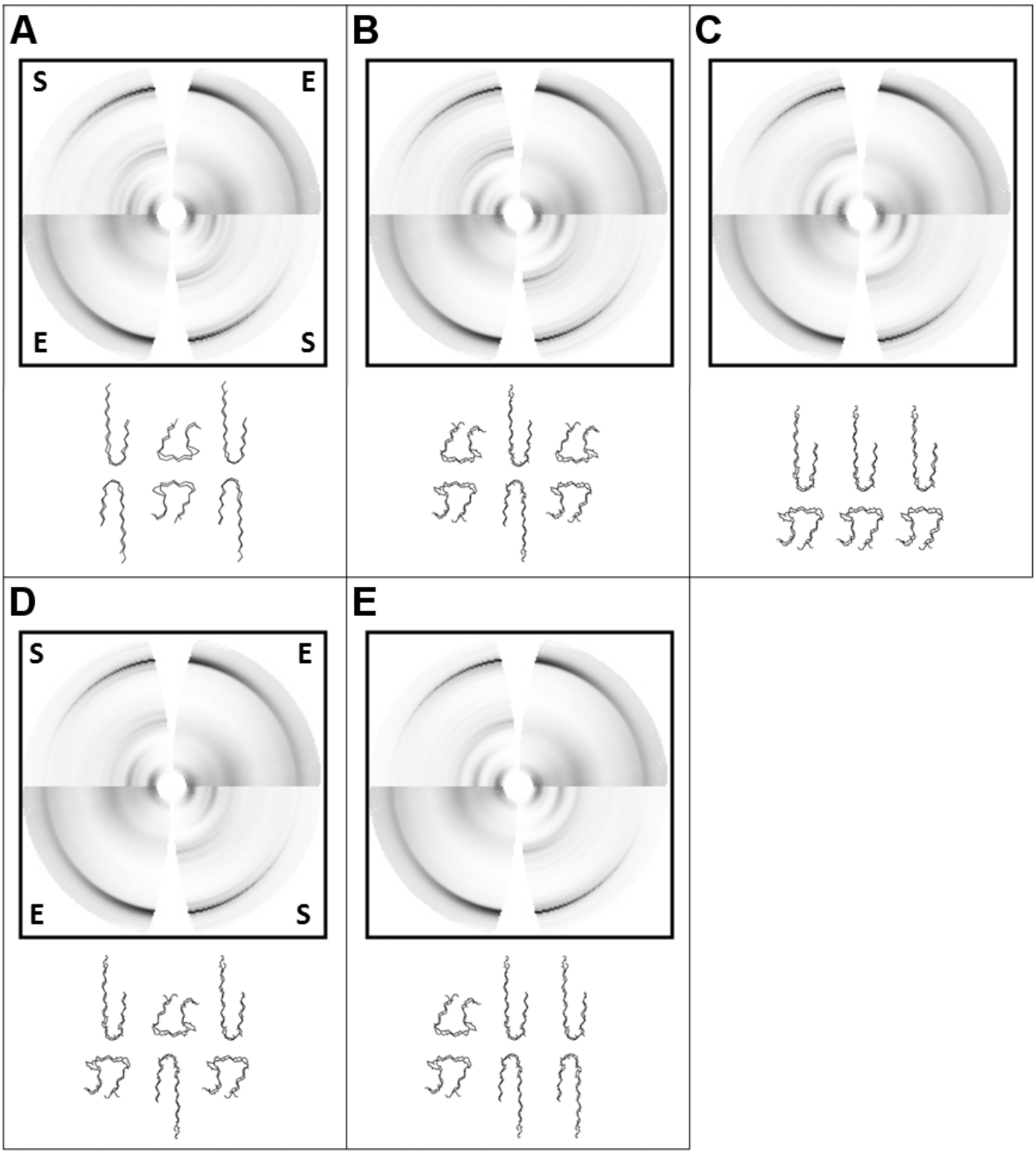

Figure S6. Experimental diffraction pattern of an insulin amyloid fibril and simulated diffraction patterns of hybrid models of β-roll and β-helix–based twisted stack fibrils. (**A**-**E**) Each panel shows the cross-section of a model with a quadrant view of the experimental insulin X-ray fiber diffraction pattern (E) and the simulated fiber diffraction pattern (S).

8. Supplementary Figure 7

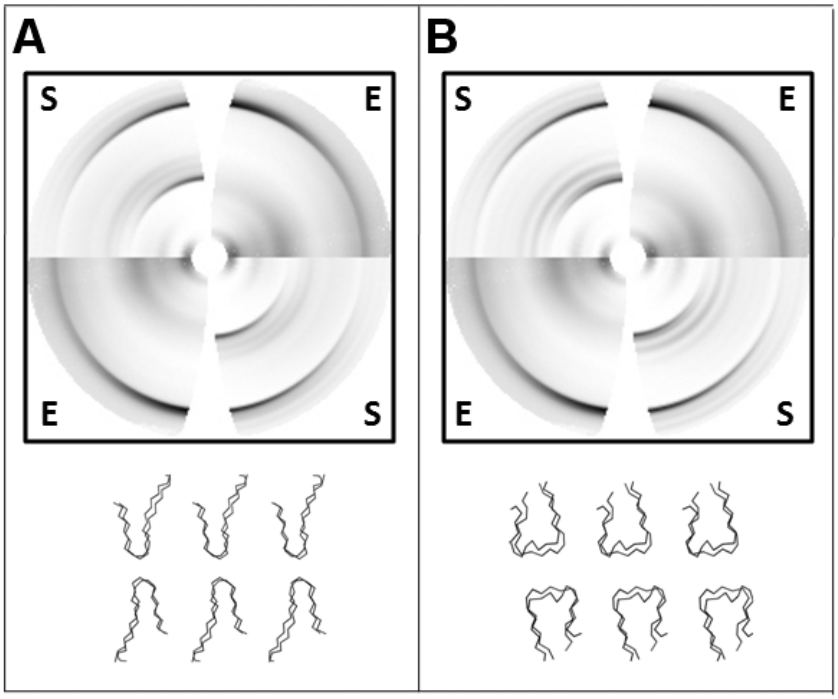

Figure S7. Experimental diffraction pattern of an insulin amyloid fibril and simulated diffraction patterns of β-roll and β-helix twisted stack fibril models built based on final structures of MD simulations. (**A-B**) Each panel shows the cross-section of a model with a quadrant view of the experimental insulin X-ray fiber diffraction pattern (E) and the simulated fiber diffraction pattern (S).

9. Supplementary Table 2

Table S2. Least-squares residuals and the parameters of the optimized models.

Type	Model[a]	Number of proto-filaments	Period[b] (Å)	Axial translation[c] (Å)	Turns[d]	Units[e]	α_0[f]	k_{solv}[g]	B_{sol}[h]	B[i]	R_{md}[j]	R_{eq}[k]	R[l]
β-roll	S3-A	2	525	9.4	1	56	25	0.98	1479.03	3.00	0.24	0.55	0.47
	S3-B	2	525	9.4	1	56	25	0.98	924.53	9.47	0.22	0.77	0.50
	S3-C	2	525	9.4	1	56	25	0.99	1553.15	6.82	0.20	0.46	0.39
	S3-D	4	355	9.4	1	38	25	0.97	1596.31	9.20	0.24	0.53	0.46
	S3-E	6	426	9.4	1	45	25	0.99	1175.65	9.90	0.21	0.33	0.37
β-helix	S4-A	2	525	9.4	1	56	25	0.98	799.64	2.00	0.42	0.60	0.56
	S4-B	2	525	9.4	1	56	25	0.98	764.61	3.43	0.38	0.62	0.54
	S4-C	2	525	9.4	1	56	25	0.99	1220.32	2.46	0.37	0.43	0.49
	S4-D	4	355	9.4	1	38	25	0.96	831.36	2.84	0.47	0.39	0.53
	S4-E	6	426	9.4	1	45	25	0.94	785.18	2.09	0.36	0.32	0.42
Hybrid models of β-roll and β-helix													
Hybrid	S6-A	6	426	9.4	1	45	25	0.99	1286.22	2.64	0.29	0.14	0.25
	S6-B	6	426	9.4	1	45	25	0.99	1034.71	2.01	0.31	0.21	0.26
	S6-C	6	426	9.4	1	45	25	0.99	1107.93	2.10	0.30	0.16	0.28
	S6-D	6	426	9.4	1	45	25	0.98	1157.90	2.40	0.29	0.18	0.24
	S6-E	6	426	9.4	1	45	25	0.95	873.12	8.34	0.33	0.18	0.30
Models based on MD final structures – 15 ns													
β-roll	S7-A	6	426	9.4	1	45	25	0.92	1572.82	9.35	0.45	0.34	0.41
β-helix	S7-B	6	426	9.4	1	45	25	0.94	1577.21	9.44	0.59	0.28	0.79

[a]Models were shown in Fig. S3, S4, S6 and S7. [b]Values were taken from Jimenez et al. (1). [c]The axial translation of symmetrically related units on the helix in (Å). [d]Number of helical turns in period. [e]Number of units in period, U ≅ Period (Å) / Axial translation (Å). [f]The disorientation parameter. [g,h]Optimized bulk solvent parameters. [i]Optimized model atoms isotropic temperature factor. The least-squares residuals for [i]meridional and [k]equatorial reflection regions and for [l]whole diffraction pattern were calculated using the DISORDER program (2).

10. Supplementary Table 3

Table S3. Least-squares residuals and the parameters of the optimized β-helix-based helical fibril models.

Type	Model[a]	Number of proto-filaments	Period[b] (Å)	Axial translation[c] (Å)	Turns[d]	Units[e]	α_0[f]	k_{solv}[g]	B_{sol}[h]	B[i]	R_{md}[j]	R_{eq}[k]	R[l]
β-helix (multi-fold)	S5-A	3	268	3.2	28	84	25	0.97	816.67	3.83	0.25	0.57	0.45
	S5-B	4	268	2.4	28	112	25	0.95	750.23	2.23	0.26	0.65	0.47
	S5-C	5	268	1.9	28	140	25	0.95	950.00	2.50	0.25	0.66	0.47
	S5-D	6	268	1.6	28	168	25	0.99	1552.59	5.05	0.29	0.59	0.46
	S5-E	8	268	1.2	28	224	25	0.99	799.83	2.22	0.27	0.76	0.49

[a]Models were shown in Fig. S5. [b]Values were taken from Vestergaard et al. (3). [c]The axial translation of symmetrically related units on the helix in (Å), A ≅ Period / U (number of units in period). [d]Number of helical turns in period, T ≅ Period / 9.4 Å. [e]Number of units in period, U ≅ T × (Number of symmetrical fold). [f]The disorientation parameter. [g,h]Optimized bulk solvent parameters. [i]Optimized model atoms isotropic temperature factor. The least-squares residuals for [i]meridional and [k]equatorial arc regions and for [l]whole diffraction pattern were calculated using the DISORDER program (2).

11. Supplementary Figure 8

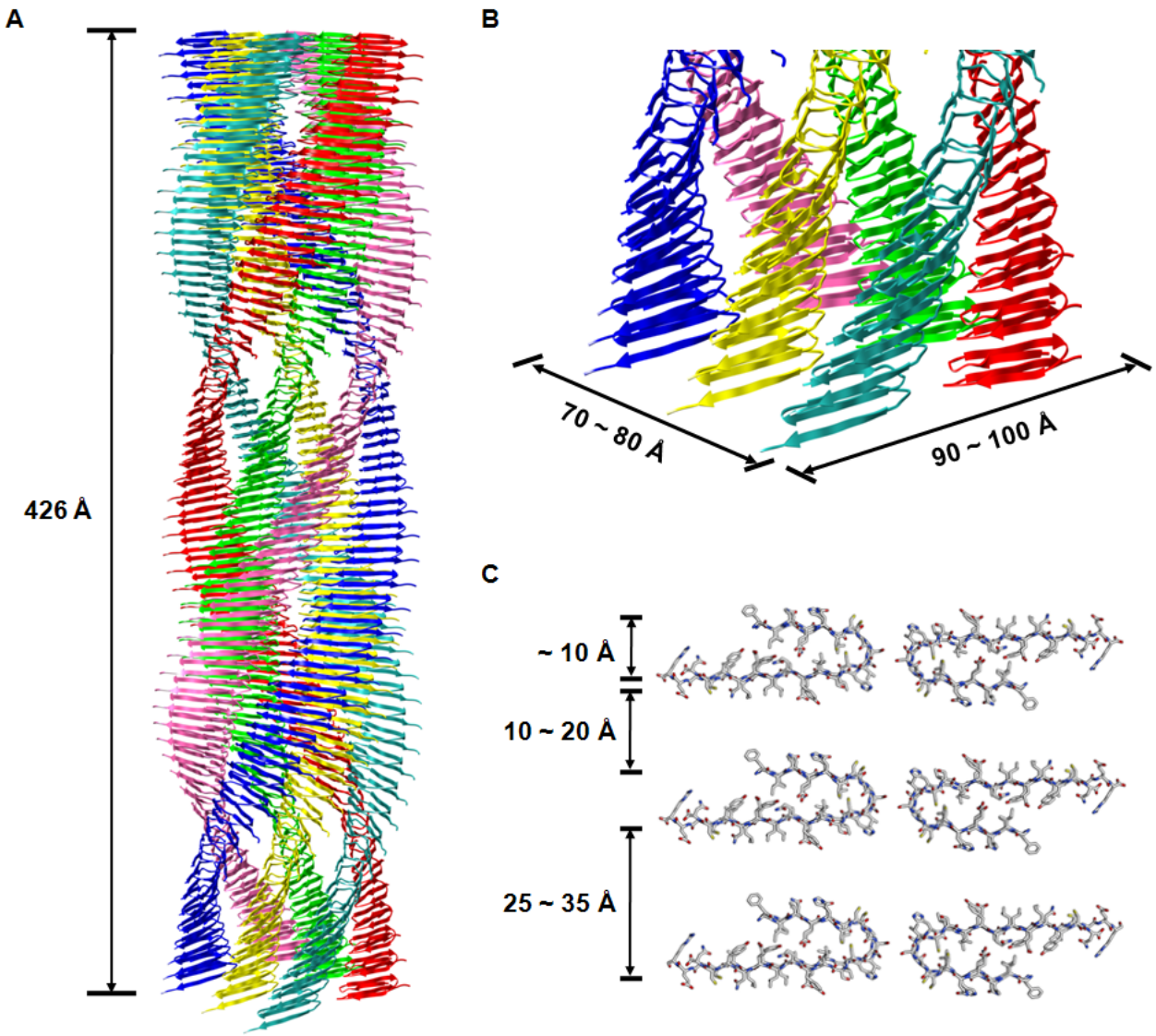

Figure S8. : Six-protofilament β-roll-based insulin fibril model. (**A**) six-protofilament β-roll-based insulin fibril model with a helical period of 426 Å. (**B**) the close-up view of the fibril model and estimated dimensions of the cross-section. (**C**) Cross-sectional view with estimated distances of peptide chains within and between β-roll subunits.

12. METHODS: Moecular modeling, molecular dynamic simulation, and fiber diffraction simulation of the insulin monomeric subunit and insulin fibril.

Molecular modeling of the insulin monomer

The β-roll and β-helix models of C-terminally truncated human insulin (A chain: 1-21 and B chain: 1-22) were built using the iron transporter stabilizer protein SufD (Protein Data Bank [PDB] ID code: 1VH4) and the C-terminal domain of *N*-acetyglucosamine 1-phosphate uridyltransferase GlmU (PDB ID code: 1HV9) as templates. For the β-roll model, the structural coordinates from residues 254-274 and 230-249 of 1VH4 were copied and reassembled onto the scaffold so as to follow the selected threading of the insulin A and B chains, respectively (see Results). For the β-helix model, the coordinates from residues 309-323 and 293-312 of 1HV9 were used to build the A and B chains, respectively. The backbone chains were refined by relocating C_α of the cysteine residues (A chain: residues 6, 7, 11, and 20 and B chain: residues 7 and 19) to satisfy the disulfide bond constraints. The side chains of the insulin sequence were subsequently placed using InsightII software (4). For the β-helical model, the loop region of chain A (residues 7-10) was built using PLOP (5). The side chain positions of both models were subsequently optimized using SCWRL 3.1 (6). Both models were optimized using two rounds of energy minimization using the GROMACS 3.1.3 package (7). β-roll and β-helix polymeric models were constructed by stacking four repeated subunits on top of each other with an intermolecular distance between two neighboring subunits of 4.8 Å.

Molecular dynamics simulation of monomeric insulin models

All simulations were performed with the GROMACS software package (7), using the GROMMOS 43a3 force field (8), as described in previous studies (9, 10). The model structures used in the simulations were the C-terminally truncated β-roll and β-helix insulin. Models were solvated individually in octahedron boxes filled with water molecules (11). A single point charge water model was used for the solvent molecules in the simulation (12). Sodium ions were used to electroneutralize the system. Solutes, solvent, and counterions were coupled independently to reference temperature baths at 300 K, 345 K, and 375 K (13), and the pressure was maintained by weakly coupling the system to an external pressure bath at 1 atm (9). Bond lengths were constrained by the LINCS procedure (14) and non-bonded interactions were evaluated using twin-range cut-offs of 0.8 and 1.4 nm for the Lennard-Jones and Coulomb potentials. Long-range electrostatic interactions beyond the cut-offs were treated with the generalized reaction field model, using a dielectric constant of 54 (9). The integration time step was set to 0.002 ps and the trajectory coordinates and energies were stored at 0.5 ps intervals. To emulate the acidic, fibrillogenic condition of pH ~2, two histidine residues, one glutamate residue, and the C-terminus were protonated. Analysis was performed using the built-in programs of the GROMACS software package (7).

Molecular modeling of the insulin fibril

Two types of fiber models were explored using β-solenoid monomeric units; 1) a twisted stack arrangement (Fig. S3 & S4) and 2) a helical architecture (Fig. S5), based on previous Cryo-EM (1) and SAXS (3) data respectively.

For twisted stack fibril models (S3A-S3E in Fig. S3 and S4A-S4E in Fig. S4), each model of a fibril cross-section was constructed by translating the β-roll or β-helix monomeric units in the direction perpendicular to the fibril axis and rotating around the fiber axis. The

resulting models of fibril cross-sections were used as inputs to DISORDER (2) as helical asymmetric units. Finally, fibril models with β-sheets twisting along the fiber axis were constructed in DISORDER using helical parameters, as described in Table S2. For helical fibril models (S5A-S5E in Fig. S5), models were constructed from a β-helical subunit based on the helical parameters (Table S3), estimated from the SAXS data (3).

Fiber diffraction simulations of the insulin fibril

The simulation and analysis of fiber diffraction patterns were conducted using DISORDER (2). For every fibril model, the diffraction patterns, with varying degrees of disorientation between fibrils, were simulated. The value of the disorientation parameter varied from 10-25°. The meridional and equatorial profiles of the simulated and experimental fiber diffraction patterns were then compared by calculating the least-squares residuals (2). Simulated and experimental diffraction patterns were visualized using FIT2D (15).

An image of the experimental insulin fiber diffraction pattern was kindly provided by Dr. Minna Groenning. This image was previously captured using insulin amyloid grown from human insulin (5 mg/ml) in 20% acetic acid (pH 2.0), with 0.5 M sodium chloride at 45 °C. The X-ray diffraction pattern was collected at a synchrotron source at 20 °C; λ=1.3 Å, and a 350-mm specimen:detector distance during a 30 s exposure (3). The diffraction pattern was preprocessed to subtract the background noise and to build a quadrant view image using the FibreFix software package (16). Selected models and simulated fiber diffraction images are available at http://www.cmpharm.ucsf.edu/cohen/insulin.

Modeling positioning

The fiber axis was aligned with the direction of the z-axis of the model coordinate system. The models of the asymmetric unit were initially placed into the coordinate system so that their centers of masses were located at the origin and the average direction of the H-bonding coincided with the z-axis. The models were positioned by two rotation transformations, followed by translation along the x-axis (2).

Optimization of the model parameters by simulated annealing

To obtain a better fit of the simulated diffraction patterns to the experimental data, the bulk solvent parameters k_{solv} and B_{solv} and isotropic model *B*-factors were optimized for every model by simulated annealing minimization of the whole pattern residuals (2).

Comparison of simulated and observed diffraction patterns

The fiber diffraction residual was calculated for every model as a measure of the similarity of the simulated to the observed pattern using the least-square method (2). R, the least-square residual is calculated by summation across the whole diffraction pattern and is not limited to the layer lines. Experimental diffraction data up to 4.4 Å resolution in meridional direction and up to 6.7 Å in radial direction were used for quantitative comparison.

Processing of fiber diffraction diagrams

The insulin fiber diffraction pattern image was kindly provided by Dr. Minna Groenning. A circularly symmetric background was subtracted from the diffraction patterns using the program FibreFix (16). Data were mapped into reciprocal space using the program FTOREC (17) and stored in two-dimensional 101x101 arrays (resolution 0.0025 $Å^{-1}$/pixel). The diffracted

intensities were corrected for the circular polarization of the incident X-ray beam using program FTOREC.

REFRECNES

1. Jimenez, J. L., E. J. Nettleton, M. Bouchard, C. V. Robinson, C. M. Dobson, and H. R. Saibil. 2002. The protofilament structure of insulin amyloid fibrils. Proc Natl Acad Sci U S A 99:9196-9201.
2. Borovinskiy, A. 2006. DISORDER (http://fibernet.vanderbilt.edu/software/disorder).
3. Vestergaard, B., M. Groenning, M. Roessle, J. S. Kastrup, M. van de Weert, J. M. Flink, S. Frokjaer, M. Gajhede, and D. I. Svergun. 2007. A helical structural nucleus is the primary elongating unit of insulin amyloid fibrils. PLoS Biol 5:e134.
4. Accelrys. 2000. InsightII. San Diego, CA.
5. Jacobson, M. P., D. L. Pincus, C. S. Rapp, T. J. Day, B. Honig, D. E. Shaw, and R. A. Friesner. 2004. A hierarchical approach to all-atom protein loop prediction. Proteins 55:351-367.
6. Canutescu, A. A., A. A. Shelenkov, and R. L. Dunbrack, Jr. 2003. A graph-theory algorithm for rapid protein side-chain prediction. Protein Sci 12:2001-2014.
7. Van Der Spoel, D., E. Lindahl, B. Hess, G. Groenhof, A. E. Mark, and H. J. Berendsen. 2005. GROMACS: fast, flexible, and free. J Comput Chem 26:1701-1718.
8. Daura, X., A. E. Mark, and W. F. Van Gunsteren. 1998. Parametrization of aliphatic CHn united atoms of GROMOS96 force field. Journal of Computational Chemistry 19:535-547.
9. Langedijk, J. P., G. Fuentes, R. Boshuizen, and A. M. Bonvin. 2006. Two-rung model of a left-handed beta-helix for prions explains species barrier and strain variation in transmissible spongiform encephalopathies. J Mol Biol 360:907-920.
10. Choi, J. H., C. Govaerts, B. C. May, and F. E. Cohen. 2008. Analysis of the sequence and structural features of the left-handed beta-helical fold. Proteins 73:150-160.
11. Eisenberg, D., and A. D. McLachlan. 1986. Solvation energy in protein folding and binding. Nature 319:199-203.
12. Berendsen, H. J., J. P. Postma, W. F. van Gunsteren, and J. Hermans. 1981. Interaction models for water in relation to protein hydration. Reidel Publishing Company, Dordrecht.
13. Berendsen, H. J., J. P. M. Postma, W. F. van Gunsteren, A. DiNola, and J. R. Haak. 1984. Molecular dynamics with coupling to an external bath. Journal of Chemical Physics 81:3684-3690.
14. Hess, B., H. Bekker, J. Hermans, H. J. Berendsen, and J. G. E. M. Fraaije. 1997. LINCS: A linear constraint solver for molecular simulations. Journal of Computational Chemistry 18:1463-1472.
15. Hammersley, A. 1997. FIT2D: An Introduction and Overview. ESRF, Grenoble, France.
16. Rajkumar, G., H. Al-Khayat, F. Eakins, A. He, C. Knupp, and J. Squire. 2005. FibreFix - A New Integrated CCP13 Software Package. Fibre Diffraction Review 13:11-18.
17. Denny, R. 1993. Integration of fibre diffraction patterns: FTOREC and LSQINT. Fibre Diffraction Review 2:5-8.